Journal of Alloys and Compounds 521 (2012) 112–120

Contents lists available at SciVerse ScienceDirect

Journal of Alloys and Compounds

journal homepage: www.elsevier.com/locate/jallcom

Amorphous $Al_{1-x}Ti_x$, $Al_{1-x}V_x$, and $Al_{1-x}Fe_x$ phases in the hydrogen cycled $TiCl_3$, VCl_3 and $FeCl_3$ enhanced $NaAlH_4$ systems

M.P. Pitt[a,c,e,*], P.E. Vullum[b], M.H. Sørby[a], H. Emerich[d], M. Paskevicius[c], C.E. Buckley[c], E. MacA. Gray[e], J.C. Walmsley[b,f], R. Holmestad[b], B.C. Hauback[a]

[a] Physics Department, Institute for Energy Technology, P.O. Box 40 Kjeller N-2027 Norway
[b] Department of Physics, Norwegian University of Science and Technology, N-7491 Trondheim, Norway
[c] Department of Imaging and Applied Physics, Curtin University, GPO Box U1987, Perth 6845, Western Australia, Australia
[d] Swiss-Norwegian Beam Line, European Synchrotron Radiation Facility, BP 220, Grenoble Cedex, France
[e] Queensland Micro and Nanotechnology Centre, Griffith University, Brisbane 4111, Australia
[f] SINTEF, Materials and Chemistry, NO-7465 Trondheim, Norway

ARTICLE INFO

Article history:
Received 13 December 2011
Received in revised form 10 January 2012
Accepted 11 January 2012
Available online 28 January 2012

Keywords:
Metal hydrides
Amorphous materials
Transition metal alloys and compounds
Synchrotron radiation
Transmission electron microscopy (TEM)

ABSTRACT

The twice hydrogen (H) cycled planetary milled (PM) and cryo milled (CM) $NaAlH_4 + xTMCl_3$ (transition metal (TM) = Ti, V, Fe) systems ($x > 0.1$) have been studied by high resolution synchrotron X-ray diffraction, and high resolution transmission electron microscopy (TEM). Intense primary amorphous (a-) $Al_{1-x}TM_x$ halos are evident in diffraction data of PM samples for V and Fe, and in CM samples for Ti, V, and Fe. Weaker primary amorphous $Al_{1-x}Ti_x$ halos are evident in PM samples for Ti. The Ti poor a-$Al_{1-x}Ti_x$ phase observed for $NaAlH_4 + xTiCl_3$ ($x > 0.1$) ranges in composition from a-$Al_{86.5}Ti_{13.5}$ → a-$Al_{92}Ti_8$. High resolution TEM studies of the $Al_{1-x}V_x$ phases in the H cycled PM $NaAlH_4 + 0.1VCl_3$ system demonstrates that a nanoscopic composite morphology can exist between face centred cubic (fcc) crystalline (c-) $Al_{1-x}V_x$ and a-$Al_{1-x}V_x$ phases, with the c-$Al_{1-x}V_x$/a-$Al_{1-x}V_x$ composite embedded on the $NaAlH_4$ surface. The amorphous $Al_{1-x}V_x$ reaches ca. 28 at.% V.

1. Introduction

The transition metal enhanced $NaAlH_4$ system remains as the prototypical example of catalysis of complex hydrides. Typically, with the addition of a catalytic phase, the catalyst can be added in increasing quantities with corresponding benefit to the system until the catalytic function plateaus. Early studies of the $NaAlH_4 + xTiCl_3$ system showed that typical catalytic behavior is observed, with hydrogenation rates increasing as a function of $TiCl_3$ content [1–3], and the fastest rates being observed for 10 mol% $TiCl_3$ (ca. 31 wt.% H/hour for absorption [1]). Later studies have shown that the hydrogenation rates for low mol% $TiCl_3$ (2–4 mol%) enhanced $NaAlH_4$ can dramatically increase (up to ca. 27–65 wt.% H/hour for desorption [4,5]) if a pre-milling step utilizing Tetrahydrofuran is utilized. This suggests that poor mixing/distribution of the $TiCl_3$ additive occurs when only dry milling of $NaAlH_4 + xTiCl_3$ is performed. As such, it remains unclear if the typical catalytic behavior observed in the early studies [1–3] is an artifact of poor mixing during the milling process. Further, the hydrogenation rate can vary dramatically depending on the Ti-precursor, with 2 mol% $Ti(OBu^n)_4$ enhanced $NaAlH_4$ displaying rapid kinetics (ca. 40 wt.% H/hour [6]) immediately after milling, with no pre-treatment. The milling atmosphere is also critical, with $NaH + Al + 0.02TiCl_3$ milled under a hydrogen atmosphere displaying rapid hydrogenation kinetics (ca. 120 wt.% H/hour) immediately [7]. Presently, no study exists which follows the reduction process and observation of the formation of $Al_{1-x}Ti_x$ phases as a function of $TiCl_3$ content which could explain the variation in hydrogenation rate for $TiCl_3$ enhanced $NaAlH_4$.

In an attempt to understand the catalytic behaviour at high mol% $TiCl_3$, several studies exist that have utilised $TiCl_3$ rich samples in order to assist in the identification of $Al_{1-x}Ti_x$ species that have formed after hydrogen cycling. In [8] it was estimated from iterative quantitative analysis of synchrotron X-ray data that over 80% of Ti atoms could be accounted for in a crystalline (c-) $Al_{85}Ti_{15}$ phase in planetary milled (PM) and hydrogen cycled $NaAlH_4 + 0.1TiCl_3$. No other crystalline Ti containing phases could be observed in the diffraction data. This c-$Al_{85}Ti_{15}$ composition was later confirmed by the known concentration dependent unit cell parameters for $Al_{1-x}Ti_x$ ($x < 0.25$) in [9,10], and verified by localised

* Corresponding author at: Hydrogen Storage Research Group Department of Imaging and Applied Physics Curtin University Kent Street, Bentley Perth, WA 6102, Australia. Tel.: +61 8 9266 3673; fax: +61 8 9266 2377.
E-mail address: mark.pitt@gmail.com (M.P. Pitt).

0925-8388/$ – see front matter © 2012 Elsevier B.V. All rights reserved.
doi:10.1016/j.jallcom.2012.01.062

nano beam energy dispersive compositional analysis (EDS) and high resolution TEM images of the surface regions of twice H cycled $NaAlH_4 + 0.1TiCl_3$ in [10]. For the $NaAlH_4 + xTiCl_3$ ($x < 0.05$) system, the $Al_{1-x}Ti_x$ species formed currently remain unidentified by diffraction. However, the large difference in hydrogenation kinetics between 0.9 and 9 mol% $TiCl_3$ enhanced $NaAlH_4$ [1] suggests that different $Al_{1-x}Ti_x$ species have formed, and at the 10 mol% $TiCl_3$ level, potentially up to 20% [8] of the originally added Ti atoms exist in a non-crystalline state. An amorphous $Al_{1-x}Ti_x$ phase has been suggested to exist in cooled vibration milled $NaAlH_4 + 0.1TiCl_3$, although *d*-spacings for the maxima of the primary halo and possible Al:Ti composition are not specified [11]. The observation that the 'broad reflection' in [11] is centred in the range $2\theta = 40–41^\circ$ (for Cu Kα X-ray radiation) in-between Al (1 1 1) and Al (2 0 0) indicates the 'broad reflection' is centred in the range 2.20–2.25 Å, suggesting a Ti poor amorphous $Al_{1-x}Ti_x$ ($x < 0.25$) phase [12,13] for vibration milled $NaAlH_4 + 0.1TiCl_3$.

The potential for an amorphous Ti poor $Al_{1-x}Ti_x$ phase in 10 mol% $TiCl_3$ enhanced $NaAlH_4$ is also consistent with the studies in [14,15], which show the formation of a nanoscopic, surface embedded, crystalline Al/amorphous $Al_{50}Ti_{50}$ composite on the surface of $NaAlH_4$ after the completion of the $NaAlH_4 + 0.1TiCl_3$ milling process. The matching of the size range of the nano Al (2–20 nm) in PM $NaAlH_4 + 0.1TiCl_3$ compared with c-$Al_{85}Ti_{15}$ (4–25 nm) in H cycled $NaAlH_4 + 0.1TiCl_3$ indicates that Ti diffuses very locally from the amorphous $Al_{50}Ti_{50}$ matrix into the nanoscopic Al [10], subsequently forming nanoscopic crystalline $Al_{1-x}Ti_x$ phases. For 10 mol% $TiCl_3$ enhanced $NaAlH_4$, at least 80% [8] of the Ti atoms diffuse out of the original a-$Al_{50}Ti_{50}$ matrix to form c-$Al_{85}Ti_{15}$, realising the potential for a residual Ti poor amorphous $Al_{1-x}Ti_x$ matrix, of as yet undetermined Al:Ti composition. In this study, we aim to determine by high resolution synchrotron X-ray diffraction and TEM the structural state the ca. 20% of 'missing' Ti atoms are in for the H cycled $NaAlH_4 + 0.1TiCl_3$ system. We also study the formation of amorphous $Al_{1-x}Fe_x$ and $Al_{1-x}V_x$ phases in the 10 mol% $FeCl_3$ and VCl_3 enhanced $NaAlH_4$ systems for the purpose of a morphological comparison to the $TiCl_3$ enhanced $NaAlH_4$ system.

This paper is organised as follows: Section A analyses the reliability of the *d*-spacing and crystallisation temperature of the amorphous $Al_{1-x}Ti_x$ phase in H cycled $NaAlH_4 + xTiCl_3$, in order to determine the unknown Al:Ti ratio. Section B discusses the Rietveld methodology used to quantify the Al:Ti ratio in the a-$Al_{1-x}Ti_x$ phase in CM and H cycled $NaAlH_4 + 0.1TiCl_3$. We also show high resolution TEM images of the amorphous $Al_{1-x}V_x$ in H cycled PM $NaAlH_4 + 0.1VCl_3$. Section C then utilises the same Rietveld methodology to model the a-$Al_{1-x}Ti_x$ phase in H cycled PM $NaAlH_4 + xTiCl_3$ ($x > 0.1$) samples.

2. Experimental procedure

$NaAlH_4$ was purchased from Albemarle Corporation (LOT NO.#:22470404-01, >93% purity). All transition-metal-chloride precursors were purchased from Sigma–Aldrich Chemicals Inc. (typically >99.99% purity). At all times, all powders have been handled under inert Ar atmosphere in a dry glove box, with < 1 ppm O_2 and H_2O. Milled $NaAlH_4 + xTMCl_n$ powders were prepared in 1 g quantities in a Fritsch P7 planetary mill, with ball to powder ratio (bpr) of 20:1, at 750 rpm for a period of 1 h, and in 2 g quantities in a Spex 6750 Freezer mill, milled at intensity 15 for a period of 2 h, in a custom sealed stainless steel cryo vial, with a 32 g AISI440c impactor. Milling was performed under Ar from the glove box. Hydrogen cycling was performed in a Sieverts apparatus composed of commercial VCR components, rated to 200 bar and 600 °C. Hydrogen compressibility was modelled with the most accurate known equation of state [16], and a divided volume model was applied to accurately account for the total amount of hydrogen in the system in the presence of a temperature distribution [17]. Hydrogen cycling conditions were: absorption at 140 °C under 150 bar system pressure, and desorption at 140 °C under ultra high vacuum (<10^{-6} mbar). Both absorption and desorption were carried out over 12 h time periods. Powders were studied in the fully absorbed state typically after 2 and 5 H cycles for diffraction measurements. Powder X-ray diffraction data were recorded at the Swiss-Norwegian Beamline (SNBL) at the European Synchrotron Radiation Facility (ESRF) in Grenoble, France. Samples were contained in rotating 0.8 mm boron-silica glass capillaries. High resolution data ($\Delta d/d \sim 3 \times 10^{-4}$) was typically collected at 295 K between 5–35° 2θ, in steps of 0.003 to 0.030°, depending on the sample broadening. A wavelength of 0.4998 Å was obtained from a channel cut Si (1 1 1) monochromator. Medium resolution ($\Delta d/d \sim 3 \times 10^{-3}$) in situ annealing data were also collected on a 2-D image plate (MAR345) over the 2θ range 3–34° with step size 0.015° and exposure time of 30 s, and a wavelength of 0.7111 Å. Synchrotron X-ray diffraction patterns were analysed by the Rietveld method using RIETICA [18]. Diffraction lineshape profiles were fitted with a full Voigt function, with the instrumental shape determined by a NIST LaB_6 660a lineshape standard, further annealed to 1800 °C. Transmission electron microscopy (TEM) was performed with a JEOL 2010F field emission gun operating at 200 kV, or with a Philips CM30 operating at 100–300 kV. All TEM samples were loaded inside the glove box and transferred into the column of the microscope by two different methods: (a) An oxygen tight transfer cap was used, with the cap being removed inside a glove bag attached to the holder entrance of the microscope. The glove bag was pumped and flushed with pure N_2 to prevent sample oxidation. (b) A Gatan environmental cell TEM holder was used. A vacuum gate valve on the environmental chamber allowed the sample to be withdrawn and isolated in the chamber during transfer, which prevented contamination or contact with air. Method (a) was most frequently used. Further details regarding TEM measurements can be found in [19].

3. Results and discussion

3.1. A. The use of crystallisation temperature (T_{cryst}) and *d*-spacing to determine the Al:Ti ratio of the amorphous $Al_{1-x}Ti_x$ phase in H cycled $NaAlH_4 + xTiCl_3$ samples

Fig. 1 presents a series of diffraction patterns for the twice H cycled $NaAlH_4 + 0.1TMCl_n$ samples TM = Ti, V, and Fe, across the most interesting range of *d*-spacing from 1.9 to 2.4 Å. The data are scaled to match the (1 1 1) NaCl intensity contribution. Very broad peaks are evident for all samples except for PM $NaAlH_4 + 0.1TiCl_3$, with peak maximas occurring in the 2.04–2.21 Å *d*-spacing range. The broad peaks indicate either nanoscopic or amorphous $Al_{1-x}TM_x$ phases, dependent on the observation of further broad crystalline reflections at other *d*-spacings.

For the Ti based system, the CM $NaAlH_4 + 0.1TiCl_3$ and H cycled sample shows the most interesting feature, with an intense $Al_{1-x}Ti_x$ amorphous primary halo evident. The peak maxima is centered at a *d*-spacing of ca. 2.21 Å, at the position that primary amorphous

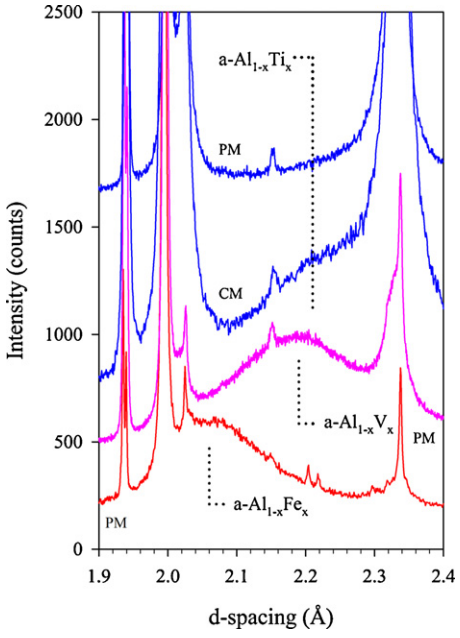

Fig. 1. Raw synchrotron X-ray data series from 1.9 to 2.4 Å for the twice H cycled $NaAlH_4 + 0.1TMCl_3$ system with TM = Ti, V, and Fe for PM samples, and Ti for CM samples. The maxima of primary amorphous halos are evident for $Al_{1-x}Fe_x$ at ca. 2.06 Å, for $Al_{1-x}V_x$ at ca. 2.19 Å, and for $Al_{1-x}Ti_x$ at ca. 2.21 Å.

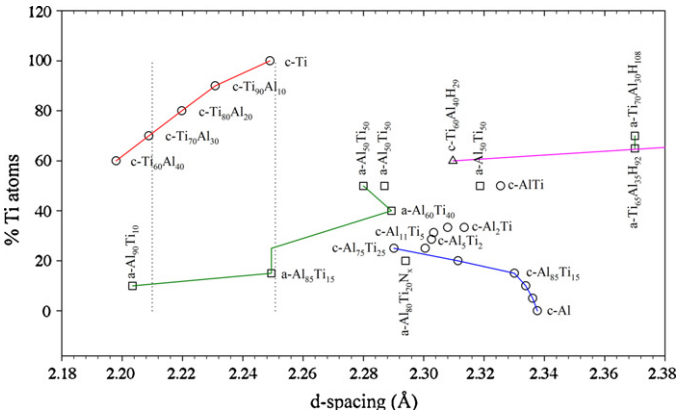

Fig. 2. The strongest X-ray diffraction intensity of all known $Al_{1-x}Ti_xH_y$ phases across the *d*-spacing range 2.18–2.38 Å.

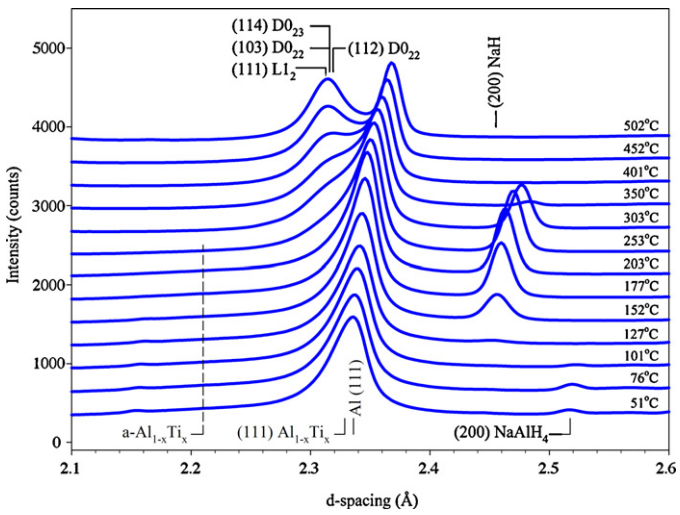

Fig. 3. In situ annealing synchrotron X-ray data for twice H cycled CM $NaAlH_4 + 0.1TiCl_3$ measured to 500 °C. The amorphous $Al_{1-x}Ti_x$ phase shows crystallisation occurring in the 250–300 °C range. Above 300 °C, the c-$Al_{86}Ti_{14}$ phase shows a clear shift to lower *d*-spacing with crystallisation of the ordered $L1_2$ Al_3Ti phase evident, with the (1 0 0) primitive reflection evident at ca. *d* = 4.00 Å. Splitting into the tetragonal $D0_{22}$ and $D0_{23}$ structures can also be clearly observed by 400 °C.

halos of binary $Al_{1-x}Ti_x$ ($x < 0.15$) phases are typically centered [12,13] (the halos for $x > 0.15$ are centered at higher *d*-spacing, as shown in Fig. 2). Shoulders are also present on the low *d*-spacing side of the Al reflections, demonstrating that the sample contains a mixture of c-$Al_{1-x}Ti_x$ + a-$Al_{1-x}Ti_x$ phases. Note that aside from the high symmetry cubic c-$Al_{1-x}Ti_x$ phase (present as shoulders on the Al) [10], there are no other visible $Al_{1-x}Ti_x$ crystalline contributions to the data at other *d*-spacings, suggesting the broad reflection at 2.21 Å is not from a nanocrystalline $Al_{1-x}Ti_x$ phase. The broad $Al_{1-x}Ti_x$ halo at 2.21 Å is so intense in the H cycled CM $NaAlH_4 + 0.1TiCl_3$ data, that if it were a c-$Al_{1-x}Ti_x$ phase, any other reflections would easily be discerned in the data, and as they are clearly not visible, we hereafter refer to the broad reflection at 2.21 Å as a primary amorphous $Al_{1-x}Ti_x$ halo. This is further supported by inspection of Fig. 2. c-$Ti_{70}Al_{30}$ and c-$Ti_{60}Al_{40}$ show intensity maxima at *d* = 2.21 and 2.20 Å, however, if these phases had formed during milling of $NaAlH_4 + xTiCl_3$, they would have hydrided during the first thermal desorption or subsequent absorption, to distinctly higher *d*-spacings representing c-$Ti_{60}Al_{40}H_{29}$ and a-$Ti_{70}Al_{30}H_{108}$ at *d* = 2.31 and 2.37 Å, respectively [20].

The *d*-spacing maxima of the $Al_{1-x}Ti_x$ primary amorphous halo is a very useful tool to estimate the unknown Al:Ti composition of the a-$Al_{1-x}Ti_x$ phase in H cycled CM $NaAlH_4 + 0.1TiCl_3$. Fig. 2 shows the variation in *d*-spacing (2.18–2.38 Å) of the strongest X-ray diffracted intensity for all known crystalline and amorphous $Al_{1-x}Ti_xH_y$ phases. These *d*-spacings have been interpolated as accurately as possible from published diffraction data in the literature. This data is generally collected with Cu Kα X-ray radiation, without specification of the zero point offset. As such, there is a minor unknown degree of uncertainty in the estimation of each *d*-spacing. c-Al to c-$Al_{75}Ti_{25}$ *d*-spacings are reported in [9], and c-Ti to c-$Ti_{60}Al_{40}$ (and their hydrides) are reported in [20]. Ordered c-Al_2Ti, c-Al_5Ti_2 and c-$Al_{11}Ti_5$ are reported in [21]. c-AlTi, a-$Al_{50}Ti_{50}$ and its hydride a-$Al_{50}Ti_{50}H_{41}$ are reported in [22]. a-$Al_{90}Ti_{10}$ is reported in [13], a-$Al_{85}Ti_{15}$ in [12], a-$Al_{60}Ti_{40}$ in [20], and a-$Al_{50}Ti_{50}$ in [12,22–25]. A review of all crystalline $Al_{1-x}Ti_x$ structures in the most recently evaluated binary Al–Ti phase diagram can be found in [26]. The hydride of a-$Al_{50}Ti_{50}$ is reported as a-$Al_{50}Ti_{50}H_{41}$ and does not show any detectable shift in *d*-spacing of the primary halo in the hydrogenated state. Pure TiH_{2-x} phases show intensity maxima at >2.5 Å. Sputter deposited and mechanically alloyed a-$Al_{50}Ti_{50}$ yield halo maximas that cover the *d*-spacing range 2.28–2.32 Å. Without knowledge of the zero offsets, it remains unclear if this halo maxima range is genuine, however, the difference in maxima position between a-$Al_{50}Ti_{50}$ and a-$Al_{90}Ti_{10}$ is quite distinct (as shown in Fig. 2). Based on the *d*-spacing of the primary halo maxima and a potential ±0.02 Å range, we expect that the halo maxima we observe at 2.21 Å for twice H cycled CM $NaAlH_4 + 0.1TiCl_3$ represents an amorphous composition a-$Al_{1-x}Ti_x$ ($x < 0.15$). We note also that the average figure of 2.30 Å for the a-$Al_{50}Ti_{50}$ halo maxima is in excellent agreement with the strongly deviated synchrotron X-ray background in CM $NaAlH_4 + 0.1TiCl_3$. The presence of the a-$Al_{50}Ti_{50}$ phase is further supported by high resolution TEM and Energy Dispersive X-ray Spectroscopy (EDS) compositional analysis showing a-$Al_{49.3}Ti_{50.7}$ for the surface embedded nano Al/a-$Al_{50}Ti_{50}$ composite [14,15]. As such, we can also state that the nanoscopic a-$Al_{1-x}Ti_x$ phases we observe embedded on the $NaAlH_4$ surface display primary halo maxima in excellent agreement with literature values for micron sized a-$Al_{1-x}Ti_x$ phases.

Traditionally, the crystallisation temperature, T_{cryst}, of an amorphous phase has also served as a reliable indicator of the elemental phase composition. Fig. 3 shows annealing diffraction data for a twice H cycled CM $NaAlH_4 + 0.1TiCl_3$ sample. The amorphous halo at *d* = 2.30 Å is observed to crystallise in the range T_{cryst} = 250–300 °C, with a significant *d*-spacing shift of c-$Al_{1-x}Ti_x$ occurring at 250 °C. A mixture of $D0_{22}$ and $D0_{23}$ ordered $Al_{75}Ti_{25}$ phases are observed at high temperature (>300 °C). The comprehensive high temperature study of $Al_{1-x}Ti_x$ phases ($Al_{95}Ti_5$ to $Al_{75}Ti_{25}$) in [9] demonstrates that if a $D0_{22}/D0_{23}$ mixture has formed at high temperature, it has crystallised from a solid solution in the range $Al_{90}Ti_{10}$ to $Al_{80}Ti_{20}$. Reported crystallisation temperatures of amorphous $Al_{1-x}Ti_x$ phases are contradictory, $Al_{90}Ti_{10}$ T_{cryst} = 307 °C, $Al_{92}Ti_8$ T_{cryst} = 277 °C (melt spins) [13], $Al_{50}Ti_{50}$ 500 °C < T_{cryst} < 600 °C, $Al_{75}Ti_{25}$ 200 °C < T_{cryst} < 350 °C, $Al_{85}Ti_{15}$ T_{cryst} = 325 °C (co-deposited thin films) [12], with [13] indicating a lowering of T_{cryst} with decreasing Ti content, and [12] indicating the opposite trend. This difficulty in correctly extracting the Al:Ti composition of the amorphous phase from crystallization temperature measurements is further compounded by the dependence of T_{cryst} on heating rate, and some authors quoting T_{cryst} at the onset of crystallisation, or as a temperature range equal to the width of the exothermic spike in DSC spectra.

In [12], a broad primary halo can be observed for the deposited a-$Al_{1-x}Ti_x$ compositions (on liquid nitrogen cooled substrates) in the 15 to 60 at.% Ti range. In general, the sputter deposit halos appear very homogenous, while at short milling times (<100 h), mechanically alloyed samples can display mixtures of crystalline

and amorphous components within the diffracted halo, such as for a-$Al_{50}Ti_{50}$, as described in [27], where a Ti(Al) solid solution reflection can be observed as a satellite on the halo. At longer milling times, the halos are homogenous [28]. No such satellites exist in our data, neither in the milled or H cycled state, and our high resolution TEM and compositional analysis indicates homogenous a-$Al_{1-x}Ti_x$ phases [14,15]. Radiation induced amorphisation of a Ti rich $Al_{78}Ti_{22}$ composition is reported in [29], but no amorphisation could be achieved for $Al_{76}Ti_{24}$. The X-ray absorption study in [30] suggests an amorphous $Al_{75}Ti_{25}$ composition occurs for milled $NaAlH_4$ + 0.02–0.04$TiCl_3$, however, a 3:1 amorphous Al:Ti composition is not plausible for a-$Al_{1-x}Ti_x$ phases based on literature for micron sized phases [28,29]. Although there exist a significant number of reports on synthesising $Al_{1-x}Ti_x$ intermetallic phases by ball milling, none have reported the existence of amorphous phases for $x = 0.25$, even after 1000 h of ball milling [28], likely due to the instability of the amorphous phase relative to the corresponding crystalline composition, as can be observed in the binary Al–Ti thermodynamic phase diagram in [31]. The composition after milling $TiCl_3$ with $NaAlH_4$ has been correctly determined as a-$Al_{50}Ti_{50}$ for CM $NaAlH_4$ + 0.1$TiCl_3$ in [14,15].

It is clear that, in general, it remains difficult to accurately determine elemental Al:Ti ratios in amorphous $Al_{1-x}Ti_x$ ($x < 0.25$) phases based on reported crystallisation temperatures, and that we must turn to other techniques to accurately quantify the Al:Ti ratio. From our compositional EDS analysis of CM $NaAlH_4$ + 0.1$TiCl_3$ in [14,15], the surface embedded amorphous phase initially shows an $Al_{50}Ti_{50}$ composition. With the formation of the majority c-$Al_{85}Ti_{15}$ phase occurring during H cycling at temperature [8,10], Ti must be sourced from the a-$Al_{50}Ti_{50}$ matrix, indicating that the amorphous matrix becomes Ti poor during thermal annealing/and or H cycling, and we expect that the final composition of the amorphous phase must be considerably Ti poor, based on the majority, >80% of Ti atoms being accounted for in the c-$Al_{85}Ti_{15}$ solid solution in PM and H cycled $NaAlH_4$ + 0.1$TiCl_3$ in [8]. In addition, the 2.21 Å *d*-spacing of the primary halo maxima and the low crystallisation temperature (of ca. 250–300 °C in our annealing data in Fig. 3) for the a-$Al_{1-x}Ti_x$ phase suggest an amorphous composition of at least $Al_{90}Ti_{10}$ based on reported crystallisation temperatures [13], and of Ti compositions of <15 at.% based on the *d*-spacing of the primary halo maximum. This a-$Al_{90}Ti_{10}$ to a-$Al_{85}Ti_{15}$ range provides an excellent starting point for the Quantitative Phase Analysis (QPA) of diffraction data presented in the next section, and is indicative of a Ti poor a-$Al_{1-x}Ti_x$ ($x < 0.15$) phase composition with a primary halo maximum of 2.21 Å in CM and H cycled $NaAlH_4$ + 0.1$TiCl_3$.

For a-$Al_{1-x}Ti_x$ phases, Fig. 2 shows an increasing *d*-spacing for the halo maxima as a function of Ti content. However, it can be noted that the a-$Al_{80}Ti_{20}$ halo maxima [32] appears out of position, at a higher than expected *d*-spacing of ca. 2.29 Å. This discrepancy can be attributed to the use of nitrogen gas during the sputtering process of the a-$Al_{80}Ti_{20}$ sample. It has long been known that large amounts (up to 50 at.%) of N can be absorbed by $Al_{1-x}Ti_x$ ($x < 0.5$) phases when milled under a N_2 atmosphere [33], and as such, the a-$Al_{80}Ti_{20}$ composition reported [32] should be properly described as a ternary nitride. While Ar is not absorbed in the same fashion as N, it has been observed that increasing Ar pressure in sputter deposited a-$Al_{50}Ti_{50}$ can nucleate c-Ti(Al) solid solution satellite reflections on the primary a-$Al_{50}Ti_{50}$ halo [34], which is similar to the short milling time samples in [27]. This raises the question of whether the *d*-spacing halo maxima of the a-$Al_{1-x}Ti_x$ phases in milled and H cycled $NaAlH_4$ + *x*$TiCl_3$ powders are shifted by the absorption of gas phase impurities from the glove box atmosphere (including minor ppm level impurities such as O_2 and H_2O). We note the following: (i) our EDS analysis on milled samples in [14,15] reveals no O signal of any significance when we focus the beam directly on a-$Al_{50}Ti_{50}$ in milled samples, or c-$Al_{85}Ti_{15}$ in H cycled samples [10], (ii) high resolution images of the a-$Al_{50}Ti_{50}$ in [14,15] do not reveal any nucleation of hexagonal Ti(Al) solid solutions that could be induced from Ar contamination, and the a-$Al_{50}Ti_{50}$ phase appears homogenous, consistent with a homogenous single phase halo in the synchrotron X-ray data, (iii) any O contamination that does occur appears to affect only the Na, resulting in the formation of slightly sub-stoichiometric Na_2O_2 [35], and (iv) without the occurrence of milling atmosphere contamination, any further possible contamination is irrelevant in the presence of high purity hydrogen (99.9999%) used for H cycling. With no evidence of contamination of the a-$Al_{50}Ti_{50}$ phase after milling under glove box Ar, and no evidence of Na_2O_2 formation in our samples, we proceed with the assumption that the amorphous $Al_{1-x}Ti_x$ phases we observe are free of contaminants, and represent only binary $Al_{1-x}Ti_x$ compositions.

3.2. B. Modelling of the primary amorphous $Al_{1-x}Ti_x$ halo in diffraction data from CM and H cycled $NaAlH_4$ + 0.1$TiCl_3$

The QPA analysis in [8] estimates that > 80% of Ti atoms can be accounted for in PM and H cycled $NaAlH_4$ + 0.1$TiCl_3$ in the solid solution phase c-$Al_{85}Ti_{15}$. The 85:15 composition has been confirmed by nano beam EDS analysis in [10]. Based on this QPA of all crystalline phases, there appears to be some 'missing' (non-crystalline) Ti in $TiCl_3$ rich PM samples. In light of the intense amorphous $Al_{1-x}Ti_x$ halo observed in our CM and H cycled $NaAlH_4$ + 0.1$TiCl_3$ sample, we have the opportunity to perform quantitative Rietveld analysis to determine the Al:Ti composition of the amorphous $Al_{1-x}Ti_x$ phase, and to look for such phases containing the 'missing' Ti in PM samples. QPA of the CM and H cycled $NaAlH_4$ + 0.1$TiCl_3$ sample utilises the method developed by Le Bail [36,37] for the quantification of SiO_2 glasses, in which the primary amorphous halo is represented by a model nanoscopic fcc phase during Rietveld refinement. This methodology has proven as accurate as Monte Carlo simulations of the amorphous component [37].

Fig. 4(a) and (b) shows a Rietveld fit to the CM and twice H cycled $NaAlH_4$ + 0.1$TiCl_3$ sample. Fig. 4(b) is a zoomed image showing the intense amorphous $Al_{1-x}Ti_x$ halo centered at 2.21 Å (ca. 13.04° 2θ for $\lambda = 0.4998$ Å). Although the c-$Al_{1-x}Ti_x$ phase in the CM data shows a broader peak shape than PM samples, it has a unit cell dimension of 4.0305 Å, yielding a c-$Al_{84}Ti_{16}$ composition based on concentration dependent lattice parameters [9], almost identical to the c-$Al_{85}Ti_{15}$ composition observed in PM samples. Our Rietveld methodology utilizes a 6 phase model with 5 known phases ($NaAlH_4$, Na_3AlH_6, Al, NaCl, and c-$Al_{86}Ti_{14}$), to determine the unknown Al:Ti ratio of the amorphous $Al_{1-x}Ti_x$ phase. As short term cryo milling is in many cases the equivalent of up to hundreds of hours of planetary milling, we also carefully checked for compression of the Al unit cell dimension, as is observed in our 48 h PM $NaAlH_4$ + 0.1$TiCl_3$ sample in [10]. No such compression is evident in our CM data, indicating different nucleation processes for $Al_{1-x}Ti_x$ phases at cryogenic temperatures. The Rietveld model is sensitive to the Al:Ti ratio in the amorphous $Al_{1-x}Ti_x$ phase, and an incorrect Al:Ti composition will yield a large overestimate of both the total Al and Ti atom count.

Our testing methodology is as follows: (i) full pattern fits were first conducted to determine the full 2θ dependent lineshape parameters of all crystalline phases, (ii) a starting background was refined for the middle of the possible Al:Ti composition range ($x < 0.25$), a-$Al_{87.5}Ti_{12.5}$, and tests were conducted with this fixed background for all compositions tested, and then tests were repeated with a refined background for all compositions (such tests are necessary due to the very broad nature of the primary halo and the direct correlation of its intensity with the placement of the background), (iii) 'half' pattern tests (with shape parameters from the full 2θ range) were then conducted up to 14 degrees 2θ to

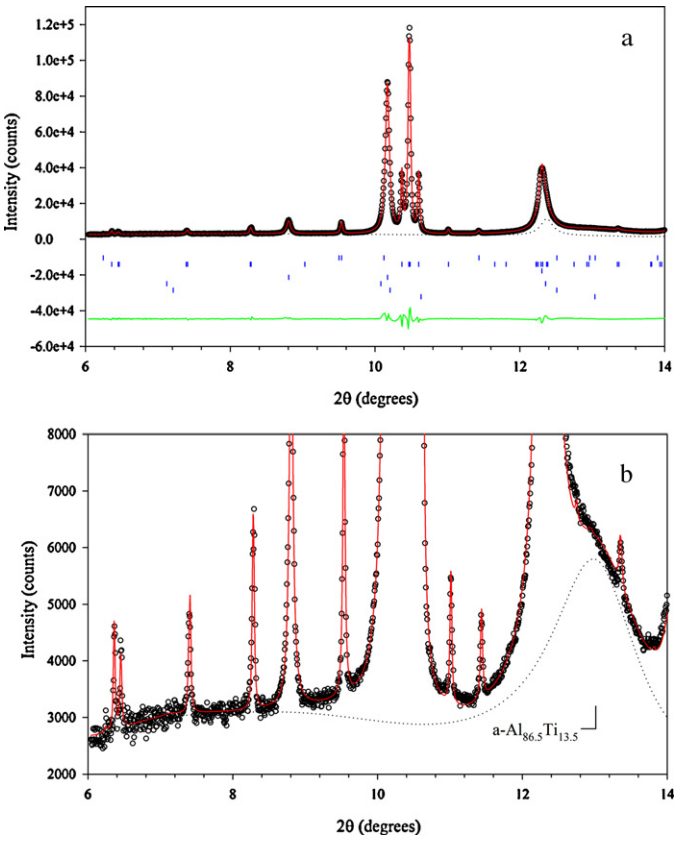

Fig. 4. (a) Final '1/2 pattern' Rietveld fit to synchrotron X-ray diffraction data of twice H cycled CM $NaAlH_4 + 0.1TiCl_3$. The dashed line shows the intensity contribution from the c-$Al_{84}Ti_{16}$ solid solution. (b) Zoomed image of (a) showing the maxima of the intense amorphous halo centred at ca. 2.21 Å (ca. 13.04° 2θ). The dashed line shows the calculated intensity contribution from a-$Al_{86.5}Ti_{13.5}$.

determine the final Al:Ti ratio in the amorphous phase, as the fcc model for the amorphous phase contributes intensity at (2 0 0) etc., where there is none, and the intensity contribution of the extremely broad and weak secondary amorphous halo (maxima centered at ca. $d = 1.35$ Å), resulting in an increased background at higher 2θ, is removed.

QPA of the total atom count of all atomic species (Na, Al, H, Cl and Ti) in the H cycled CM $NaAlH_4 + 0.1TiCl_3$ sample tested all possible Al:Ti compositions for the amorphous $Al_{1-x}Ti_x$ phase. The Al and Ti atom count for the a-$Al_{1-x}Ti_x$ phase are intrinsically correlated in the refinement as they are present in the same structure, however, the unknown Al:Ti ratio is constrained by mixing the Al and Ti on (0 0 0) of the fcc model for the a-$Al_{1-x}Ti_x$ phase such that the total occupancy n of the site is related by $n_{Ti} = n - n_{Al}$. The final determination of the Al:Ti ratio for the a-$Al_{1-x}Ti_x$ phase includes 100% of the unaccounted Ti atoms (Ti atoms not present in crystalline phases) for an a-$Al_{86.5}Ti_{13.5}$ composition. In this model of the a-$Al_{1-x}Ti_x$ phase, the total Al content is ca. 10% overestimated. The overcount of Al atoms can be removed by modeling the amorphous phase as $Al_{86.5-x}Ti_{13.5}$. However, renormalization of $Al_{86.5-x}Ti_{13.5}$ at 100% Al atoms yields a-$Al_{81}Ti_{19}$, which exists at significantly higher d-spacing than observed in Fig. 4(b). As such, renormalization of the Al count must be treated carefully, and an incorrect Al:Ti composition can result in a-$Al_{1-x}Ti_x$ at an incorrect d-spacing. The Na atom count is consistent at ca. 0.8 atoms, lower than the expected 1.0 atoms. However, the $NaAlH_4$ phase fraction is lower than expected, at ca. 1.5 mol%, and may artefactually affect the total Na atom count. If this is not the true origin of the missing ca. 0.2 Na atoms, then we must consider the dispersion of a small fraction of Na to either the microstructure or as an amorphous composition. All Cl atoms appear present at ca. 0.3 atoms for the NaCl phase, indicating complete reduction has occurred. Accepting the 10% Al overestimate and 20% Na underestimate as a mathematical artifact of the modeling process of the amorphous $Al_{1-x}Ti_x$ phase, we report the amorphous Al:Ti ratio as a-$Al_{86.5}Ti_{13.5}$ in CM and H cycled $NaAlH_4 + 0.1TiCl_3$. We note that the a-$Al_{86.5}Ti_{13.5}$ composition determined by QPA without renormalization falls in the expected a-$Al_{90}Ti_{10}$ (by T_{cryst}) to a-$Al_{85}Ti_{15}$ (by d-spacing) range determined in section A.

We have not been able to gain a high resolution TEM image that shows the amorphous $Al_{1-x}Ti_x$ phase in H cycled $NaAlH_4 + xTiCl_3$ samples clearly, however, when we focus the electron beam directly on c-$Al_{84}Ti_{16}$ crystallites, the integrated electron diffraction pattern always shows the presence of the amorphous halo at $d = 2.21$ Å [19]. This suggests a complex local surface embedded morphology between the c-$Al_{84}Ti_{16}$ and a-$Al_{86.5}Ti_{13.5}$ phases, and it is likely that the c-$Al_{84}Ti_{16}$ phase morphologically covers the a-$Al_{86.5}Ti_{13.5}$ phase. Final QPA of the diffraction data demonstrates the a-$Al_{86.5}Ti_{13.5}$ phase holds ca. 71% of the originally added Ti atoms, with the remaining 29% of Ti atoms bound within the c-$Al_{84}Ti_{16}$ solid solution. It should be emphasised that we never observe free Ti (or TiH_2) in the CM samples, in our synchrotron X-ray data, or in our localised integrated electron diffraction patterns. It is clear that it is possible in the manner described above to account for 100% of the original Ti added to H cycled CM $NaAlH_4 + xTiCl_3$.

For the H cycled VCl_3 and $FeCl_3$ enhanced $NaAlH_4$ systems, we have been able to directly observe a-$Al_{1-x}V_x$ and a-$Al_{1-x}Fe_x$ phases by TEM, corresponding to the primary halos observed in the synchrotron X-ray data in Fig. 1. Inspection of Fig. 1 shows a broad amorphous halo for the twice H cycled PM $NaAlH_4 + 0.1FeCl_3$ sample. The maxima of the primary halo occurs at a d-spacing of ca. 2.060 Å. It has been reported that a-$Al_{1-x}Fe_x$ phases will form with as little as 5 at.% Fe [38,39]. Interpolation from published data (with no knowledge of zero point offset) over a 15–42 at.% range of Fe concentration results in a d-spacing for the primary halo maximum of 2.055 Å for 15–17 at.% Fe [40], 2.059 Å for 25 at.% Fe [41], and 2.078 Å for 42 at.% Fe [42]. Notable asymmetry is evident on the primary halos at shorter milling times due to unreacted Al, and as such, the interpolated maxima quoted above may shift slightly upon complete consumption of the Al. Based on the interpolated maxima, we expect the primary halo we observe at ca. 2.060 Å is representative of a-$Al_{1-x}Fe_x$ ($x < 0.25$). For the twice H cycled PM $NaAlH_4 + 0.1FeCl_3$ sample, the amorphous $Al_{1-x}Fe_x$ phase contains all of the originally added Fe (no other crystalline Fe containing phases are present), and can be understood to be the dominant phase when inspecting the thermodynamic binary Al–Fe phase diagram in [43], which suggests the c-$Al_{1-x}Fe_x$ solid solution is thermodynamically unstable with respect to the a-$Al_{1-x}Fe_x$ phase, an opposite trend to the Al–Ti system [31]. High resolution images of the a-$Al_{1-x}Fe_x$ phase are shown in our earlier TEM studies in [19]. EDS directly on the amorphous layer indicates ca. a-$Al_{66}Fe_{34}$, while on an area containing nano Al crystallites, the average composition is ca. $Al_{85}Fe_{15}$. A similar Rietveld modeling process (to that utilized above) can be carried out on the synchrotron X-ray data to determine the Al:Fe ratio in the amorphous $Al_{1-x}Fe_x$ phase. Final analysis indicates a-$Al_{88.5}Fe_{11.5}$, which is considerably Fe poorer than the composition determined by EDS. However, the d-spacing of 2.060 Å is very close to the a-$Al_{85}Fe_{15}$ composition reported at 2.055 Å in [40], and as such, we expect that EDS measurements directly on the a-$Al_{1-x}Fe_x$ phase over several hundred particles will reveal a significant variation in a-$Al_{1-x}Fe_x$ composition, which will likely average out to the composition determined by QPA, and be in the vicinity of 15 at.% Fe.

We have also directly observed the amorphous $Al_{1-x}V_x$ phase in twice H cycled PM $NaAlH_4 + 0.1VCl_3$ by high resolution TEM, corresponding to the primary halo with maximum at ca. $d = 2.19$ Å

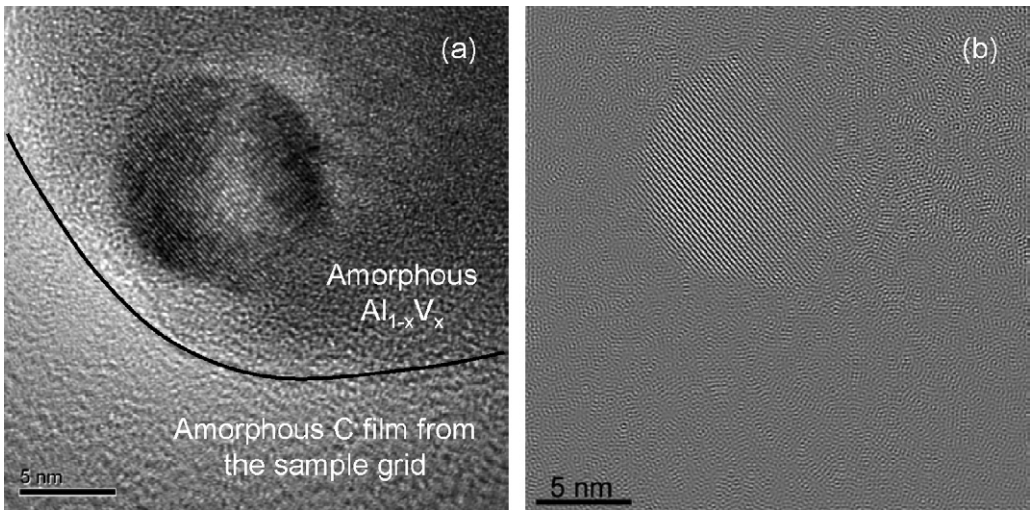

Fig. 5. High resolution TEM image of the surface region of twice H cycled PM $NaAlH_4 + 0.1VCl_3$. In (a), a ca. 12 nm c-$Al_{1-x}V_x$ crystallite is embedded in a surrounding amorphous a-$Al_{1-x}V_x$ matrix, with an inverse Fourier transformed image shown in (b) to allow easier observation of the surrounding amorphous matrix. The sample edge is delineated with a solid black line in (a).

in Fig. 1. Fig. 5(a) and (b) shows high resolution TEM images of nanocrystalline $Al_{1-x}V_x$ particles embedded in an amorphous $Al_{1-x}V_x$ matrix, on the surface of H cycled PM $NaAlH_4 + 0.1VCl_3$. Fig. 5(b) is an inverse Fourier transform of the image in (a), with the inelastic contribution filtered out. Local EDS on the crystalline phase gives an average composition of ca. c-$Al_{70}V_{30}$, while the amorphous phase ranges in composition from a-$\{Al_{77}V_{23} \leftrightarrow Al_{69}V_{31}\}$ by EDS. It initially appears that both the amorphous and crystalline phases have an Al:V composition of ca. 70:30. It is stated in [44] that amorphous phases do not form for the binary Al–V system, on the basis that only icosahedral quasicrystalline $Al_{1-x}V_x$ phases are observed to form at <18.at.% V content for melt spun ribbons in [45] and [46]. As such, our observation of amorphous $Al_{1-x}V_x$ appears to be unique, and we note that the composition we observe is > 18 at.% V, and we do not observe 5-fold symmetry in our electron diffraction data that would indicate the phase is quasicrystalline. From the study of mechanically milled $Al_{1-x}V_x$ powder mixtures in [47], no amorphous $Al_{1-x}V_x$ phases are observed. Rather, single phase crystalline extended fcc Al(V) and body centred cubic (bcc) V(Al) solid solutions are observed, with a maximum single phase composition of $Al_{90}V_{10}$ reported for the fcc solid solution, yielding a decrease of the lattice parameter 'of the order of 1%' (the exact magnitude of the contraction is not specified) compared to pure Al. The mechanical milling study in [47] indicates the maximum solubility of V in fcc Al is ca. 10 at.%. Above 10 at.% V, multiple phases are observed. Indexing of the shoulders on the low *d*-spacing side of Al reflections from our twice H cycled PM $NaAlH_4 + 0.1VCl_3$ data yields an fcc cell with dimension $a = 4.0281$ Å, which is a contraction of 0.52% compared to the Al unit cell of 4.0490 Å, and is also a decrease that is 'of the order of 1%'. Early reports on rapidly quenched binary $A_{1-x}V_x$ melts showed a contraction of the solid solution fcc unit cell of 0.10% for 0.65 at.% V in [48], and a contraction of 0.17% for 1.81 at.% V in [49]. It is well known that mechanical milling can achieve significantly higher super saturated solid solutions for fcc $Al_{1-x}TM_x$ phases, such as the case for Ti [9]. From this perspective, it is not surprising to observe a composition of $Al_{90}V_{10}$. As the exact unit cell dimension for c-$Al_{90}V_{10}$ is specified only as a contraction 'of the order of 1%' in [47], and as our indexed unit cell lies within this range, we assume a maximum c-$Al_{90}V_{10}$ composition in an A1 structure type. Rietveld QPA modeling of our twice H cycled PM $NaAlH_4 + 0.1VCl_3$ data with a fixed c-$Al_{90}V_{10}$ composition to determine the unknown Al:V ratio in the a-$Al_{1-x}V_x$ phase yields a-$Al_{72}V_{28}$, in excellent agreement with the a-$Al_{70}V_{30}$ determined by local EDS. This suggests that the c-$Al_{70}V_{30}$ composition determined by local EDS for the fcc solid solution is an artifact, and it is highly likely that the EDS signal primarily comes from the V rich amorphous matrix, and secondly from the V-poor crystalline nanoparticles embedded within the amorphous matrix. We note also that the c-$Al_{90}V_{10}$ phase is dislocation free, in contrast to the high ⟨1 1 0⟩ edge dislocation density of ca. $7.20 \times 10^{16}/m^2$ observed in the c-$Al_{86}Ti_{14}$ solid solution in H cycled CM $NaAlH_4 + 0.1TiCl_3$ [10], likely because of its smaller size < 12 nm. All of the originally added V atoms are 100% accounted for, and distributed across c-$Al_{90}V_{10}$:a-$Al_{72}V_{28}$ as 13.5%:86.5%. Such a broad $Al_{1-x}V_x$ halo (as shown at $d = 2.19$ Å in Fig. 1) has also been observed in the PM $LiAlD_4 + xVCl_3$ system at a similar *d*-spacing [50]. Only two of the known ordered Al-V intermetallics [51] possess the strongest diffracted X-ray intensity in the vicinity of 2.19 Å, $Al_{10}V$ with $d = 2.1859$ Å [52], and AlV_3 with $d = 2.2023$ Å [53]. However, strong reflections corresponding to these phases at other *d*-spacings are not observed, and our direct high resolution TEM images are compelling evidence for the formation of amorphous $Al_{1-x}V_x$. The fact that we have for the first time observed binary amorphous $Al_{1-x}V_x$ phase may be related to its very small size, ca. 10 nm, and the fact that it is well dispersed and present as isolated particles that are embedded on the $NaAlH_4$ surface. Such small sizes and an isolated morphology are not possible to achieve in rapidly quenched melts (typically microns thick) or mechanically milled powder samples.

The layered morphology between c-$Al_{90}V_{10}$ and a-$Al_{72}V_{28}$, and the similar morphology for c-$Al_{1-x}Ti_x$/a-$Al_{1-x}Ti_x$ phases implied by high resolution synchrotron X-ray data, high resolution TEM, and integrated electron diffraction data demonstrates that localized nano beam EDS on either the crystalline or amorphous $Al_{1-x}TM_x$ phase may produce an artefactual Al:TM ratio that is dependent on (a) the presence of one or both crystalline and amorphous $Al_{1-x}TM_x$ phases, (b) the relative thickness and hence contribution of each phase, and (c) the number of c-$Al_{1-x}TM_x$/a-$Al_{1-x}TM_x$ composites that are observed. A large statistical sampling by localized nano beam EDS is clearly necessary to obtain an average representative Al:TM composition for points (a) to (c), and to obtain good agreement for the a-$Al_{1-x}TM_x$ composition determined by QPA from the synchrotron X-ray data. For the particular case of amorphous $Al_{1-x}Fe_x$ where all Fe is present in the amorphous phase, we expect that the average Al:Fe composition determined by QPA from the synchrotron X-ray data is not affected by points (a) to (c). For the

particular case of Ti where we have not been able to directly observe the a-$Al_{1-x}Ti_x$ phase by high resolution TEM and obtain a large statistical sampling of the Al:Ti composition by localized nano beam EDS, the use of *d*-spacing maxima (Fig. 2) and the known concentration dependent unit cell dimensions for the fcc c-$Al_{1-x}Ti_x$ phase [9] allows an accurate deduction of the unknown a-$Al_{1-x}Ti_x$ phase composition by QPA of the synchrotron X-ray data. We note also that the a-$Al_{86.5}Ti_{13.5}$ composition determined without excess Al renormalization is consistent with similar micron sized a-$Al_{1-x}Ti_x$ phases displaying halo maxima in the vicinity of 2.21 Å [12,13], as shown in Fig. 2.

3.3. C. Amorphous and crystalline $Al_{1-x}Ti_x$ phases in PM and H cycled $NaAlH_4 + xTiCl_3$ ($x < 0.15$)

In this section, we focus on locating the 'missing Ti' in $TiCl_3$ rich H cycled PM $NaAlH_4 + xTiCl_3$ samples ($x > 0.1$). With no Ti trapped in any bulk $NaAlH_4$ microstructure [14], no Ti solubility in the $NaAlH_4$ crystal structure [35,54] and all originally added Ti accountable as a combination of crystalline and amorphous $Al_{1-x}Ti_x$ phases in H cycled CM $NaAlH_4 + 0.1TiCl_3$, we focus on the 2.21 Å region in diffraction data to determine if a similar a-$Al_{1-x}Ti_x$ phase exists for PM systems.

For both the CM and PM twice H cycled $NaAlH_4 + 0.1TiCl_3$ samples, we have not been able to obtain TEM images clearly locating the amorphous $Al_{1-x}Ti_x$ phase. It therefore remains unclear if the crystalline and amorphous $Al_{1-x}Ti_x$ phases are able to exist together in a composite morphology, or if the phases are physically separated (and we have missed observing isolated a-$Al_{1-x}Ti_x$ particles due to a small statistical sampling). Considering the starting conditions observed in milled samples where 2–20 nm Al is embedded in an amorphous $Al_{50}Ti_{50}$ matrix embedded on the $NaAlH_4$ surface [14], with local diffusion of Ti into the Al nano crystals forming 4–25 nm c-$Al_{1-x}Ti_x$ [10], a composite crystalline/amorphous $Al_{1-x}Ti_x$ morphology appears mechanically highly likely, similar to the case for V described above in section B. As we have not directly observed the a-$Al_{1-x}Ti_x$ phase by TEM, the most plausible explanation of its location is that it lies morphologically behind the c-$Al_{1-x}Ti_x$ phase, i.e., the a-$Al_{1-x}Ti_x$ is located in-between $NaAlH_4$ and c-$Al_{1-x}Ti_x$. In twice H cycled CM $NaAlH_4 + 0.1TiCl_3$ samples, localised integrated electron diffraction patterns (<150 nm selected area aperture) always show the presence of the amorphous phase at $d = 2.21$ Å. Such integrated electron diffraction patterns appear very similar to those described for our H cycled PM $NaAlH_4 + 0.1TiCl_3$ samples reported in [19]. It is clear that the 'missing Ti' in H cycled PM $NaAlH_4 + 0.1TiCl_3$ samples is bound and present as amorphous $Al_{1-x}Ti_x$. Out of 22 integrated electron diffraction patterns from the twice H cycled PM $NaAlH_4 + 0.1TiCl_3$ sample, we clearly observe the amorphous $Al_{1-x}Ti_x$ primary halo 4 times. We expect that the Ti poor amorphous $Al_{1-x}Ti_x$ composition has stabilized after a few H cycles, as it can be observed in Fig. 6 that during the 5th absorption of hydrogen by PM $NaAlH_4 + 0.1TiCl_3$, the c-$Al_{85}Ti_{15}$ does not change composition or phase proportion, nor does it absorb hydrogen, indicating no further Ti is accepted from the amorphous $Al_{1-x}Ti_x$ phase to build the fcc c-$Al_{1-x}Ti_x$ solid solution. This has also been observed during the 4th dehydrogenation [55], where no change in unit cell dimension of the c-$Al_{85}Ti_{15}$ phase can be discerned.

Close examination of the synchrotron X-ray diffraction pattern for PM and twice H cycled $NaAlH_4 + 0.1TiCl_3$ in Fig. 1 shows that the low *d*-spacing tail of the c-$Al_{85}Ti_{15}$ solid solution is clearly asymmetrically deviated around 2.21 Å, exactly where the primary halo of the amorphous phase is observed in our twice H cycled CM $NaAlH_4 + 0.1TiCl_3$ sample. This feature is readily observable when comparing it to data that has strong amorphous halos at the same *d*-spacing. However, analyzing the PM and twice H cycled $NaAlH_4 + 0.1TiCl_3$ data on its own could easily overlook the presence of the amorphous $Al_{1-x}Ti_x$ primary halo due to its low intensity. The CM diffraction data is clearly beneficial in this respect, as the a-$Al_{1-x}Ti_x$ primary halo is easily discernable. Fig. 7 compares PM 5, 10 and 15 mol% $TiCl_3$ enhanced $NaAlH_4$ after two H cycles. The a-$Al_{1-x}Ti_x$ primary halo in H cycled PM $NaAlH_4 + 0.15TiCl_3$ is readily observable, indicating that the quantitative proportion of the amorphous $Al_{1-x}Ti_x$ phase in PM samples increases as a function of Ti content. The same type of QPA testing model used in section B has been used to study the Al:Ti ratios in the amorphous $Al_{1-x}Ti_x$ phase in twice H cycled 5, 10, and 15 mol% $TiCl_3$ enhanced $NaAlH_4$. In the initial calculated models, a strong residual under-fit could be observed at ca. 2.30 Å, in the low *d*-spacing tail of the c-$Al_{85}Ti_{15}$ phase. Such a *d*-spacing corresponds to a unit cell of 3.9663 Å, consistent with the ordered $L1_2$ Al_3Ti composition. Fig. 8 shows a multi-plot of the H cycled 15 mol% $TiCl_3$ enhanced $NaAlH_4$ synchrotron X-ray diffraction data, showing the calculation with (a) c-$Al_{85}Ti_{15}$ only, (b) c-$Al_{85}Ti_{15}$ and $L1_2$ Al_3Ti only, (c) c-$Al_{85}Ti_{15}$ and a-$Al_{1-x}Ti_x$ only, and (d) c-$Al_{85}Ti_{15}$ with a mixture of $L1_2$ Al_3Ti and a-$Al_{1-x}Ti_x$. Significant under-fit remains in the low *d*-spacing tail of the c-$Al_{85}Ti_{15}$ solid solution (ca. 12.53° 2θ) if the $L1_2$ Al_3Ti phase is not included in the calculations.

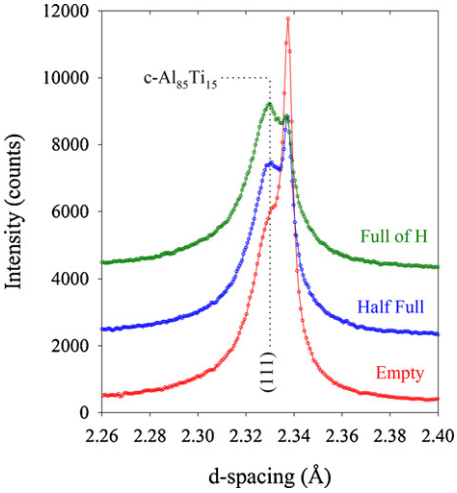

Fig. 6. The *d*-spacing of the (1 1 1) X-ray reflection of the c-$Al_{85}Ti_{15}$ solid solution (indicated by the dashed line), empty, half-full, and full of H during the 5th H absorption of PM $NaAlH_4 + 0.1TiCl_3$.

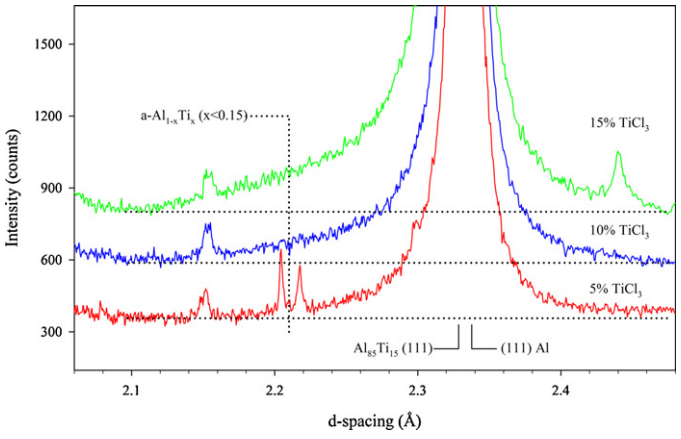

Fig. 7. Synchrotron X-ray diffraction data immediately around the 2.21 Å *d*-spacing, showing twice H cycled 5%, 10%, and 15 mol% $TiCl_3$ enhanced $NaAlH_4$. The a-$Al_{1-x}Ti_x$ phase is clearly evident in the 15% sample, with a weaker halo evident at 10% $TiCl_3$ additive level.

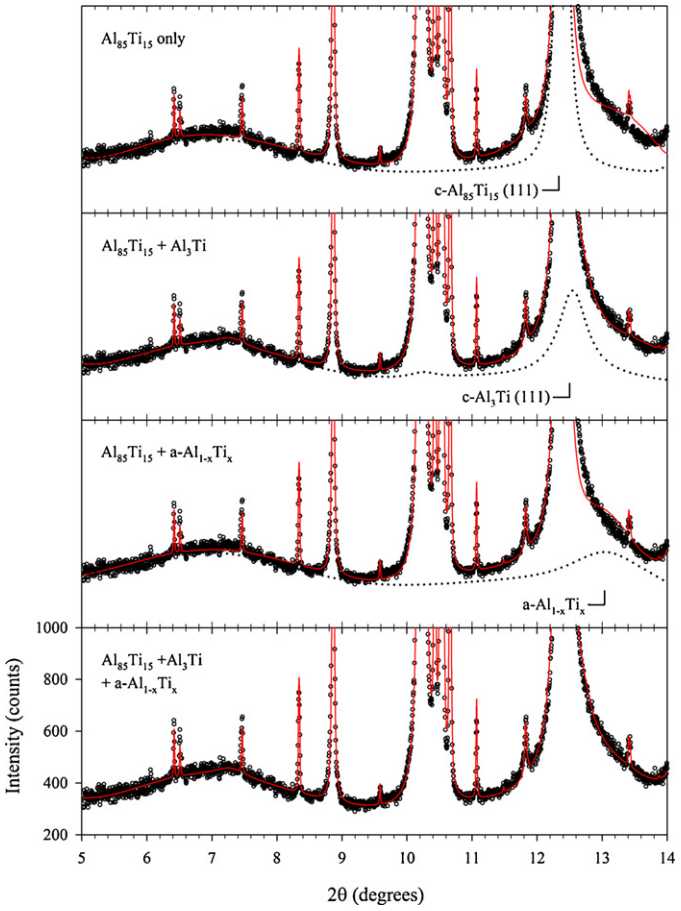

Fig. 8. Multi-plot of synchrotron X-ray data demonstrating the intensity contributions from c-$Al_{85}Ti_{15}$ and c-Al_3Ti required to produce an accurate model of the primary amorphous $Al_{1-x}Ti_x$ halo in twice H cycled PM $NaAlH_4 + 0.15TiCl_3$.

QPA of the 4 different models described above was performed for both 10 and 15 mol% $TiCl_3$ enhanced samples. By itself, c-$Al_{85}Ti_{15}$ can account for 79% of the originally added Ti atoms in PM and H cycled $NaAlH_4 + 0.15TiCl_3$, and 92% of the originally added Ti atoms in PM and H cycled $NaAlH_4 + 0.1TiCl_3$. It is clear from our integrated electron diffraction patterns that a-$Al_{1-x}Ti_x$ exists in our H cycled PM $NaAlH_4 + 0.1TiCl_3$ sample [19], and the same halo is evident with stronger intensity in the synchrotron X-ray data for the 15 mol% $TiCl_3$ enhanced $NaAlH_4$ sample in Fig. 7. It is also likely by the misfit in our calculated diffraction patterns at ca. $d = 2.30$ Å (ca. 12.50° 2θ for $\lambda = 0.5006$ Å in Fig. 8) that c-Al_3Ti is also present in our samples. We focused initially on our 15 mol% $TiCl_3$ sample with the more intense amorphous halo. c-$Al_{85}Ti_{15}$ and $L1_2$ Al_3Ti together in the 15% $TiCl_3$ sample can account for 100% of the originally added Ti atoms, however, it is clear that the low d-spacing tail of the $L1_2$ Al_3Ti phase struggles to fit the intensity contribution of the primary halo centered at 2.21 Å. The 3-phase model including c-$Al_{85}Ti_{15}$, c-Al_3Ti, and a-$Al_{1-x}Ti_x$ was tested across the range $0 < x < 25$ at.% Ti to determine the unknown Al:Ti ratio in the amorphous phase. The final composition range determined of the amorphous phases for the 10 and 15 mol% $TiCl_3$ enhanced $NaAlH_4$ samples are a-$\{Al_{98}Ti_2 \leftrightarrow Al_{96.1}Ti_{3.9}\}$, and a-$\{Al_{96}Ti_4 \leftrightarrow Al_{95.2}Ti_{4.8}\}$ respectively (including renormalization of any excess Al). It appears likely that the a-$Al_{1-x}Ti_x$ composition in the 10 and 15 mol% samples is identical. The split of Ti atoms across c-$Al_{85}Ti_{15}$, c-Al_3Ti, and a-$Al_{1-x}Ti_x$ is 59.3%;33.6%;7.1% for the 15% $TiCl_3$ sample, and 77.1%;19.2%;3.7% for the 10 mol% $TiCl_3$ sample. We note also that although we have modeled the c-Al_3Ti phase as an ordered $L1_2$ structure, this phase can also be found in the disordered A1 structure type [10]. Without verification of the existence of ordering reflections such as (1 0 0), which cannot be observed at such a low intensity, either the $L1_2$ or A1 model can be used, and both models contain an equivalent number of Ti atoms. Little literature exists describing micron sized a-$Al_{1-x}Ti_x$ phases for < 10 at.% Ti, and [13] suggests the minimum Ti content for the formation of a-$Al_{1-x}Ti_x$ phases from melt spins is 8–10 at.%. On this basis, the validity of < 5 at.% Ti a-$Al_{1-x}Ti_x$ phases in H cycled $NaAlH_4 + xTiCl_3$ is unlikely, and it is clear that our QPA analysis (ca. $Al_{96}Ti_4$) is below the suggested limiting composition of amorphous $Al_{92}Ti_8$. On the basis of [13], we then state that the a-$Al_{1-x}Ti_x$ ($x < 0.15$) phase in 10 and 15 mol% $TiCl_3$ enhanced $NaAlH_4$ is a limiting a-$Al_{92}Ti_8$ composition. Modeling the primary a-$Al_{1-x}Ti_x$ halo as a-$Al_{92}Ti_8$ changes the split of Ti atoms across c-$Al_{85}Ti_{15}$, c-Al_3Ti, and a-$Al_{92}Ti_8$ only slightly to 55.9%;31.2%;12.9% for the 15 mol% $TiCl_3$ sample, and 72.6%;18.7%;8.7% for the 10 mol% $TiCl_3$ enhanced $NaAlH_4$ sample.

4. Conclusion

Amorphous, Ti poor, $Al_{1-x}Ti_x$ ($x < 0.15$) phases can be observed in the H cycled PM $NaAlH_4 + xTiCl_3$ system at rich $TiCl_3$ contents > 10 mol%. The Ti poor a-$Al_{1-x}Ti_x$ phase ranges in composition from a-$Al_{86.5}Ti_{13.5}$ → a-$Al_{92}Ti_8$. While we have not been able to directly observe the a-$Al_{1-x}Ti_x$ phase by high resolution TEM, it always appears together with the fcc c-$Al_{1-x}Ti_x$ solid solution phase in integrated electron diffraction patterns of the immediate surface regions. Supporting evidence from the H cycled $FeCl_3$ and VCl_3 enhanced $NaAlH_4$ systems shows that (i) amorphous $Al_{1-x}Fe_x$ phases exist as 6–13 nm thick layers embedded on the $NaAlH_4$ surface, and (ii) small <12 nm $Al_{90}V_{10}$ crystallites are embedded within an amorphous $Al_{72}V_{28}$ matrix as a composite morphology on the $NaAlH_4$ surface. Such features suggest that for the Ti system, it is highly likely that a-$Al_{1-x}Ti_x$ is covered by c-$Al_{1-x}Ti_x$ in a nanoscopic morphologically layered c-$Al_{1-x}Ti_x$/a-$Al_{1-x}Ti_x$ composite that is embedded on the $NaAlH_4$ surface.

Acknowledgements

This work was supported by the Synchrotron Program of the Research Council of Norway. MPP thanks the staff of the Swiss-Norwegian Beam Line for providing experimental assistance and logistics during long-term attachments.

References

[1] G. Sandrock, K. Gross, G. Thomas, J. Alloys Compd. 339 (2002) 299–308.
[2] K.J. Gross, E.H. Majzoub, S.W. Spangler, J. Alloys Compd. 356–357 (2003) 423–428.
[3] W. Luo, K.J. Gross, J. Alloys Compd. 385 (2004) 224–231.
[4] T. ProzoroV, J. Wang, A.D. Ebner, J.A. Ritter, J. Alloys Compd. 419 (2006) 162–171.
[5] T. Wang, J. Wang, A.D. Ebner, J.A. Ritter, J. Alloys Compd. 450 (2008) 293–300.
[6] D. Sun, S.S. Srinivasan, G. Chen, C.M. Jensen, J. Alloys Compd. 373 (2004) 265–269.
[7] M.P. Pitt, M. Paskevicius, C.J. Webb, M.H. Sorby, S. Delleda, T.R. Jensen, B.C. Hauback, C.E. Buckley, E.M. Gray, Int. J. Hydrogen Energy 36 (2011) 8403–8411.
[8] H.W. Brinks, B.C. Hauback, S.S. Srinivasan, C.M. Jensen, J. Phys. Chem. B 109 (2005) 15780–15785.
[9] M. Schoenitz, Z. Xiaoying, E.L. Dreizin, J. Meta. Nanocryst. Mater. 20–21 (2004) 455–461.
[10] M.P. Pitt, P.E. Vullum, M.H. Sorby, M.P. Sulic, C.M. Jensen, J.C. Walmsley, R. Holmestad, B.C. Hauback, Acta Mater. 56 (2008) 4691–4701.
[11] A.G. Haiduc, H.A. Stil, M.A. Schwarz, P. Paulus, J.J.C. Geerlings, J. Alloys Compd. 393 (2005) 252–263.
[12] D.E. Mencer, D.G. Naugle Jr., D.L. Cocke, Appl. Phys. Commun. 11 (1992) 7–18.
[13] H. Kimura, K. Sasamori, A. Inoue, Mater. Trans. JIM 39 (1998) 773–777.
[14] M.P. Pitt, P.E. Vullum, M.H. Sorby, D. Blanchard, M.P. Sulic, H. Emerich, M. Paskevicius, C.E. Buckley, J.C. Walmsley, R. Holmestad, B.C. Hauback, J. Alloys Compd. 513 (2012) 597–605.
[15] M.P. Pitt, P.E. Vullum, M.H. Sorby, D. Blanchard, M.P. Sulic, H. Emerich, M. Paskevicius, C.E. Buckley, J.C. Walmsley, R. Holmestad, B.C. Hauback, J. Alloys Compd. 514 (2012) 163–169.

[16] K.G. McLennan, E.M. Gray, Meas. Sci. Technol. 15 (2004) 211–215.
[17] E.M. Gray, in: G. Walker (Ed.), Solid-state Hydrogen Storage: Materials and Chemistry, Woodhead Publishing, London, 2008.
[18] B.A. Hunter, Communications in Powder Diffraction Newsletter 20 (1998) 21.
[19] P.E. Vullum, M.P. Pitt, J.C. Walmsley, B.C. Hauback, R. Holmestad, J. Alloys Compd. 509 (2011) 281–289.
[20] K. Hashi, K. Ishikawa, K. Suzuki, K. Aoki, J. Alloys Compd. 330–332 (2002) 547–550.
[21] J.C. Schuster, H. Ipser, Z. Metall. 81 (1990) 389–396.
[22] K. Hashi, K. Ishikawa, K. Suzuki, A. Kiyoshi, Mater. Trans. JIM 43 (2002) 2734–2740.
[23] M.R. Farhang, A.R. Kamali, M. Nazarian-Samani, Mater. Sci. Eng. B 168 (2010) 136–141.
[24] N. Forouzanmehr, F. Karimzadeh, M.H. Enayati, J. Alloys Compd. 471 (2009) 93–97.
[25] S.Z. Wang, G. Shao, P. Tsakiropoulos, F. Wang, Mater. Sci. Eng. A 329–331 (2002) 141–146.
[26] J.C. Schuster, M. Palm, J. Phase Equilib. Diffus. 27 (2006) 255–277.
[27] M. Oehring, T. Klassen, R. Bormann, J. Mater. Res. 8 (1993) 2819–2829.
[28] T. Itsukaichi, K. Masuyama, M. Umemoto, I. Okane, J.G. Cabanas-Moreno, J. Mater. Res. 8 (1993) 1817–1828.
[29] K. Kyllesbech Larsen, S. Skovmand, N. Karpe, J. Bottiger, R. Bormann, Nucl. Instrum. Methods Phys. Res. Sect. B 80–81 (1993) 390–393.
[30] J. Graetz, J.J. Reilly, J. Johnson, A.Y. IgnatoV, T.A. Tyson, Appl. Phys. Lett. 85 (2004) 500.
[31] M. Oehring, Z.H. Yan, T. Klassen, R. Bormann, Phys. Status Solidi A 131 (1992) 671–689.
[32] A. Inoue, H. Yamagata, T. Masumoto, Mater. Lett. 16 (1993) 181–184.
[33] M. Miki, T. Yamasaki, Y. Ogino, Mater. Trans. JIM 34 (1993) 952–959.
[34] M. Chinmulgund, R.B. Inturi, J.A. Barnard, Thin Solid Films 270 (1995) 260–263.
[35] H.W. Brinks, C.M. Jensen, S.S. Srinivasan, B.C. Hauback, D. Blanchard, K. Murphy, J. Alloys Compd. 376 (2004) 215–221.
[36] A. Le Bail, J. Non-Cryst. Solids 183 (1995) 39–42.
[37] L. Lutteroti, R. Ceccato, R. Dal Maschio, E. Pagani, Mater. Sci. Forum 278–281 (1998) 87–92.
[38] T. Mukai, S. Suresh, K. Kita, H. Sasaki, N. Kobayashi, K. Higashi, A. Inoue, Acta Mater. 51 (2003) 4197–4208.
[39] H. Sasaki, K. Kita, J. Nagahora, A. Inoue, Mater. Trans. JIM 42 (2001) 1561–1565.
[40] M. Krasnowski, T. Kulik, Mater. Chem. Phys. 116 (2009) 631–637.
[41] H.W. Sheng, Y.H. Zhao, Z.Q. Hu, K. Lu, Phys. Rev. B: Condens. Matter Mater. Phys. 56 (1997) 2302–2305.
[42] B. Huang, K.N. Ishihara, P.H. Shingu, Mater. Sci. Eng. A 231 (1997) 72–79.
[43] D.K. Mukhopadhyay, C. Suryanarayana, F.H. Froes, Metall. Mater. Trans. A 26 (1995) 1939–1946.
[44] A. Inoue, H.M. Kimura, K. Sasamori, T. Masumoto, Nanostruct. Mater. 7 (1996) 363–382.
[45] K.V. Rao, J. Fidler, H.S. Chen, Europhys. Lett. 1 (1986) 647–653.
[46] A. Inoue, L. Arnberg, B. Lehtinen, M. Oguchi, T. Masumoto, Metall. Trans. A 17 (1986) 1657–1664.
[47] F. Cardellini, V. Contini, G. Mazzone, Philos. Mag. A 78 (1998) 1021–1035.
[48] N.I. Varich, L.M. BuroV, K.Y. Kolesnichenko, A.P. Maksimenko, Phys. Metals Metall. 15 (1963) 111–113.
[49] M. Moss, Acta Metall. 16 (1968) 321–326.
[50] D. Blanchard, A.I. Lem, S. Overgaard, H.W. Brinks, B.C. Hauback, J. Alloys Compd. 458 (2008) 467–473.
[51] B. Huber, K.W. Richter, J. Alloys Compd. 493 (2010) L33–L35.
[52] A.D. Caplin, L.K. Nicholson, J. Phys. F: Met. Phys. 8 (1978) 51–73.
[53] H. Holleck, F. Benesovsky, H. Nowotny, Monatshefte für Chemie 94 (1963) 477–481.
[54] O.M. Lovvik, S.M. Opalka, Phys. Rev. B: Condens. Matter Mater. Phys. 71 (2005) 054103.
[55] H.W. Brinks, M. Sulic, C.M. Jensen, B.C. Hauback, J. Phys. Chem. B 110 (2006) 2740–2745.